LETTERS

Synthetic magnetic fields for ultracold neutral atoms

Y.-J. Lin[1], R. L. Compton[1], K. Jiménez-García[1,2], J. V. Porto[1] & I. B. Spielman[1]

Neutral atomic Bose condensates and degenerate Fermi gases have been used to realize important many-body phenomena in their most simple and essential forms[1–3], without many of the complexities usually associated with material systems. However, the charge neutrality of these systems presents an apparent limitation—a wide range of intriguing phenomena arise from the Lorentz force for charged particles in a magnetic field, such as the fractional quantum Hall effect in two-dimensional electron systems[4,5]. The limitation can be circumvented by exploiting the equivalence of the Lorentz force and the Coriolis force to create synthetic magnetic fields in rotating neutral systems. This was demonstrated by the appearance of quantized vortices in pioneering experiments[6–9] on rotating quantum gases, a hallmark of superfluids or superconductors in a magnetic field. However, because of technical issues limiting the maximum rotation velocity, the metastable nature of the rotating state and the difficulty of applying stable rotating optical lattices, rotational approaches are not able to reach the large fields required for quantum Hall physics[10–12]. Here we experimentally realize an optically synthesized magnetic field for ultracold neutral atoms, which is evident from the appearance of vortices in our Bose–Einstein condensate. Our approach uses a spatially dependent optical coupling between internal states of the atoms, yielding a Berry's phase[13] sufficient to create large synthetic magnetic fields, and is not subject to the limitations of rotating systems. With a suitable lattice configuration, it should be possible to reach the quantum Hall regime, potentially enabling studies of topological quantum computation.

In classical electromagnetism, the Lorentz force for a particle of charge q moving with velocity $\mathbf{v}$ in a magnetic field $\mathbf{B}$ is $\mathbf{v}\times q\mathbf{B}$. In the Hamiltonian formulation of quantum mechanics, where potentials play a more central role than fields, the single-particle Hamiltonian is $\mathcal{H}=\hbar^2(\mathbf{k}-q\mathbf{A}/\hbar)^2/2m$, where $\mathbf{A}$ is the vector potential giving rise to the field $\mathbf{B}=\nabla\times\mathbf{A}$, $\hbar\mathbf{k}$ is the canonical momentum and m is the mass. In both formalisms, only the products $q\mathbf{B}$ and $q\mathbf{A}$ are important. To generate a synthetic magnetic field $\mathbf{B}^*$ for neutral atoms, we engineered a Hamiltonian with a spatially dependent vector potential $\mathbf{A}^*$ producing $\mathbf{B}^*=\nabla\times\mathbf{A}^*$.

The quantum mechanical phase is the relevant and significant quantity for charged particles in magnetic fields. A particle of charge q travelling along a closed loop acquires a phase $\phi=2\pi\Phi_B/\Phi_0$ due to the presence of magnetic field $\mathbf{B}$, where Φ_B is the enclosed magnetic flux and $\Phi_0=h/q$ is the flux quantum. A similar path-dependent phase, the Berry's phase[13], is the geometric phase acquired by a slowly moving particle adiabatically traversing a closed path in a Hamiltonian with position-dependent parameters. The Berry's phase depends only on the geometry of the parameters along the path, and is distinct from the dynamic contribution to the phase, which depends upon the speed of the motion.

The close analogy with the Berry's phase implies that properly designed position-dependent Hamiltonians for neutral particles can simulate the effect of magnetic fields on charged particles. We created such a spatially varying Hamiltonian for ultracold atoms by dressing them in an optical field that couples different spin states. The appropriate spatial dependence can originate from the laser beams' profile[10,14,15] or, as here, from a spatially dependent laser–atom detuning[16]. An advantage of this optical approach over rotating gases is that the synthetic field exists at rest in the laboratory frame, allowing all trapping potentials to be time-independent.

The large synthetic magnetic fields accessible by this approach make possible the study of unexplored bosonic quantum-Hall states, labelled by the filling factor $\nu=\Phi_B/\Phi_0$, the ratio of atom number to the number of flux quanta. The outstanding open questions in quantum-Hall physics centre on systems whose elementary quasiparticle excitations are anyons: neither bosons nor fermions. In some cases these anyons may be non-abelian, meaning that moving them about each other can implement quantum gates, which makes non-abelian anyons of great interest for this 'topological' quantum computation[17]. In electronic systems, the observed $\nu=5/2$ quantum-Hall state may be such a system, but its true nature is still uncertain[18]. In contrast, the $\nu=1$ bosonic quantum-Hall state with contact interactions has the same non-abelian anyonic excitations as the $\nu=5/2$ state in electronic systems is hoped to have[19].

To engineer a vector potential $\mathbf{A}^*=A_x^*\hat{\boldsymbol{x}}$, we illuminated a ^{87}Rb Bose–Einstein condensate (BEC) with a pair of Raman laser beams with momentum difference along $\hat{\boldsymbol{x}}$ (Fig. 1a). These coupled together the three spin states, $m_F=0$ and ±1, of the $5S_{1/2}$, $F=1$ electronic ground state (Fig. 1b), producing three dressed states whose energy–momentum dispersion relations $E_j(k_x)$ are experimentally tunable. Example dispersions are illustrated in Fig. 1c. The lowest of these, with minimum at $k_{\min}$, corresponds to a term in the Hamiltonian associated with the motion along $\hat{\boldsymbol{x}}$, namely $\mathcal{H}_x^*\approx\hbar^2(k_x-k_{\min})^2/2m^*=\hbar^2(k_x-q^*A_x^*/\hbar)^2/2m^*$, where A_x^* is an engineered vector potential that depends on an externally controlled Zeeman shift for the atom with synthetic charge q^*, and m^* is the effective mass along $\hat{\boldsymbol{x}}$. To produce the desired spatially dependent $A_x^*(y)$ (see Fig. 1d), generating $-B^*\hat{\boldsymbol{z}}=\nabla\times\mathbf{A}^*$, we applied a Zeeman shift that varied linearly along $\hat{\boldsymbol{y}}$. The resulting B^* was approximately uniform near $y=0$, at which point $A_x^*=B^*y$. (Here, the microscopic origin of the synthetic Lorentz force[20] was optical along $\hat{\boldsymbol{x}}$, depending upon the velocity along $\hat{\boldsymbol{y}}$; the force along $\hat{\boldsymbol{y}}$ was magnetic, depending upon the $\hat{\boldsymbol{x}}$ velocity.) In this way, we engineered a Hamiltonian for ultracold atoms that explicitly contained a synthetic magnetic field, with vortices in the ground state of a BEC. This is distinctly different from all existing experiments, where vortices are generated by phase imprinting[21,22], rotation[7–9], or a combination thereof[23]. Each of these earlier works presents a different means of imparting angular momentum to the system yielding rotation. Figure 1e shows an experimental image of the atoms with $B^*=0$. Figure 1f, with $B^*>0$, shows vortices. This demonstrates an observation of an optically induced synthetic magnetic field.

We created a ^{87}Rb BEC in a 1,064-nm crossed dipole trap, loaded into the lowest-energy dressed state[24] with atom number N up to

[1]Joint Quantum Institute, National Institute of Standards and Technology, and University of Maryland, Gaithersburg, Maryland, 20899, USA. [2]Departamento de Física, Centro de Investigación y Estudios Avanzados del Instituto Politécnico Nacional, México DF, 07360, México.

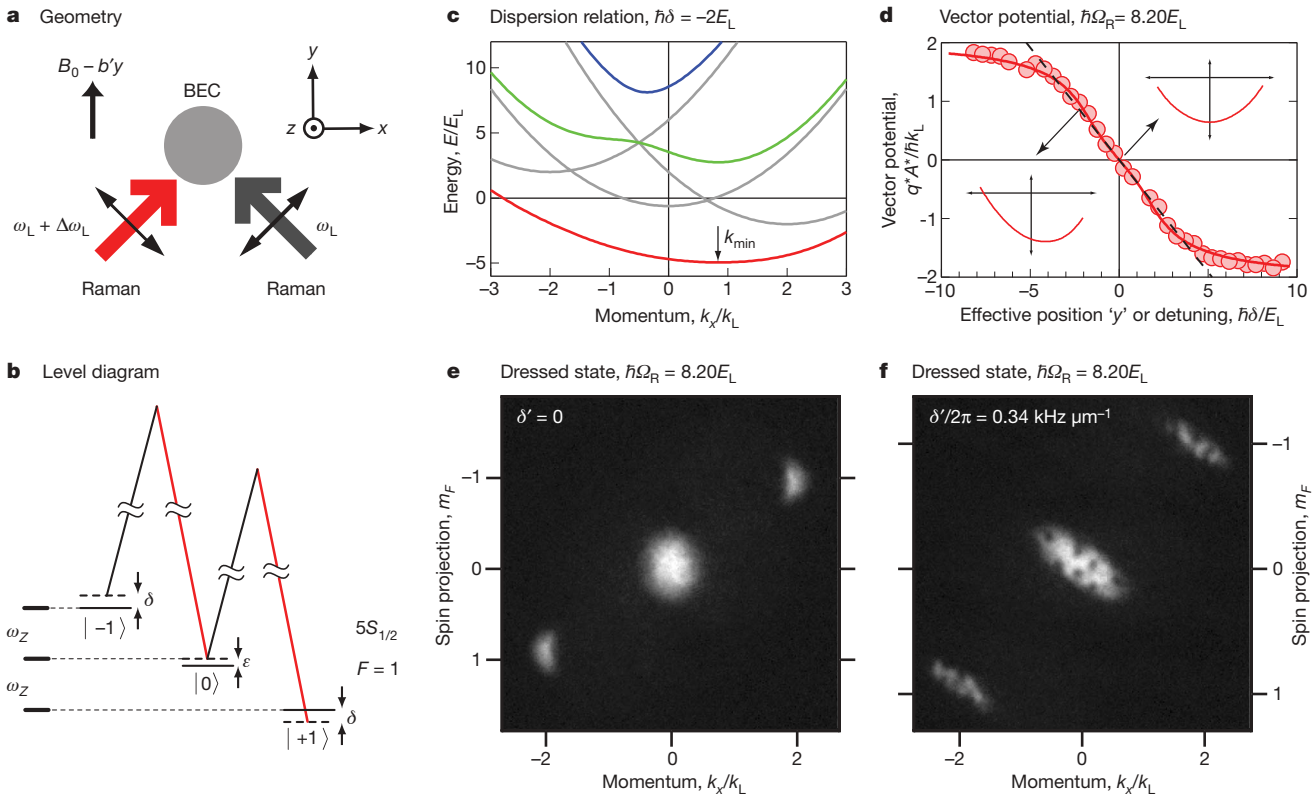

Figure 1 | Experiment summary for synthesizing magnetic fields. **a**, The BEC is in a crossed dipole trap in a magnetic field $B = (B_0 - b'y)\hat{y}$. Two Raman beams propagating along $\hat{y} \mp \hat{x}$ (linearly polarized along $\hat{y} \pm \hat{x}$) have frequencies ω_L and $\omega_L + \Delta\omega_L$. **b**, Raman coupling scheme within the $F = 1$ manifold: ω_Z and ε are the linear and quadratic Zeeman shifts, and δ is the Raman detuning. **c**, Energy–momentum dispersion relations. The grey curves represent the states without Raman coupling; the three coloured curves represent $E_j(k_x)$ of the dressed states. The arrow indicates the minimum at k_{min}. **d**, Vector potential $q^*A_x^* = \hbar k_{min}$ versus Raman detuning δ. The insets show the dispersion $E_1(k_x)$ for $\hbar\delta = 0$ (top inset) and $-2E_L$ (bottom inset). **e**, **f**, Dressed BEC imaged after a 25.1-ms TOF without (**e**) and with (**f**) a gradient. The spin components $m_F = 0$ and ± 1 separate along $\hat{y}$ owing to the Stern–Gerlach effect.

2.5×10^5, and a Zeeman shift $\omega_Z/2\pi = g\mu_B B/h \approx 2.71$ MHz, produced by a real magnetic bias field $B\hat{y}$. The $\lambda = 801.7$ nm Raman beams propagated along $\hat{y} \pm \hat{x}$ and differed in frequency by a constant $\Delta\omega_L \simeq \omega_Z$, where a small Raman detuning $\delta = \Delta\omega_L - \omega_Z$ largely determined the vector potential A_x^*. The scalar light shift from the Raman beams, combined with the dipole trap, gave an approximately symmetric three-dimensional potential, with frequencies $f_x, f_y, f_z \approx 70$ Hz. Here, $\hbar k_L = h/(\sqrt{2}\lambda)$ and $E_L = \hbar^2 k_L^2/2m$ are the appropriate units for the momentum and energy.

The spin and momentum states $|m_F, k_x\rangle$ coupled by the Raman beams can be grouped into families of states labelled by the momentum $\hbar k_x$. Each family $\Psi(k_x) = \{|-1, k_x + 2k_L\rangle, |0, k_x\rangle, |+1, k_x - 2k_L\rangle\}$ is composed of states that differ in linear momentum along $\hat{x}$ by $\pm 2\hbar k_L$, and are Raman-coupled with strength $\hbar\Omega_R$. For each k_x, the three dressed states are the eigenstates in the presence of the Raman coupling, with energies[24] $E_j(k_x)$. The resulting vector potential is tunable within the range $-2k_L < q^*A_x^*/\hbar < 2k_L$. In addition, $E_j(k_x)$ includes a scalar potential[16] V'. A_x^*, V', and m^* are functions of Raman coupling Ω_R and detuning δ, and for our typical parameters $m^* \approx 2.5m$, reducing f_x from about 70 Hz to about 40 Hz. The BEC's chemical potential $\mu/h \approx 1$ kHz is much smaller than the $\sim h \times 10$ kHz energy separation between dressed states, so the BEC only occupies the lowest-energy dressed state. Further, it justifies the harmonic expansion around $q^*A_x^*/\hbar$, valid at low energy. Hence, the complete single-atom Hamiltonian is $\mathcal{H} = \mathcal{H}_x^* + \hbar^2\left(k_y^2 + k_z^2\right)/2m + V(\mathbf{r})$, where $V(\mathbf{r})$ is the external potential including $V'(\Omega_R, \delta)$.

The dressed BEC starts in a uniform bias field $\mathrm{B} = B_0\hat{y}$, at Raman resonance ($\delta = 0$), corresponding to $A_x^* = 0$[24]. To create a synthetic field B^*, we applied a field gradient b' such that $\mathrm{B} = (B_0 - b'y)\hat{y}$, ramping in 0.3 s from $b' = 0$ to a variable value up to 0.055 Tm^{-1}, and then held it constant for t_h to allow the system to equilibrate. The detuning gradient $\delta' = g\mu_B b'/\hbar$ generates a spatial gradient in A_x^*. For the detuning range in our experiment, $\partial A_x^*/\partial\delta$ is approximately constant, leading to an approximately uniform synthetic field B^* given by $B^* = \partial A_x^*/\partial y = \delta'\partial A_x^*/\partial\delta$ (see Fig. 1d). To probe the dressed state, we switched off the dipole trap and the Raman beams in less than 1 μs, projecting each atom into spin and momentum components. We absorption-imaged the atoms after a time-of-flight (TOF) ranging from 10.1 ms to 30.1 ms (Fig. 1e, f).

For a dilute BEC in low synthetic fields, we expect to observe vortices. In this regime, the BEC is described by a macroscopic wavefunction $\psi(\mathbf{r}) = |\psi(\mathbf{r})|e^{i\phi(\mathbf{r})}$, which obeys the Gross–Pitaevskii equation (GPE). The phase ϕ winds by 2π around each vortex, with amplitude $|\psi| = 0$ at the vortex centre. The magnetic flux Φ_{B^*} results in N_v vortices and for an infinite, zero-temperature system, the vortices are arrayed in a lattice[25] with density q^*B^*/h. For finite systems vortices are energetically less favourable, and their areal density is below this asymptotic value, decreasing to zero at a critical field B_c^*. For a cylindrically symmetric BEC, B_c^* is given by $q^*B_c^*/h = 5/(2\pi R^2)\ln(0.67R/\xi)$ where R is the Thomas–Fermi radius and ξ is the healing length[26]. B_c^* is larger for smaller systems. For our non-cylindrically symmetric system, we numerically solve the GPE to determine B_c^* for our experimental parameters (see Methods).

For synthetic fields greater than the critical value, we observed vortices that enter the condensate and reach an equilibrium vortex number N_v after about 0.5 s. Owing to a shear force along $\hat{x}$ when the Raman beams are turned off, the nearly symmetric *in situ* atom cloud tilts during TOF. Although the vortices' positions may rearrange, any initial order is not lost. During the time of our experiment, the

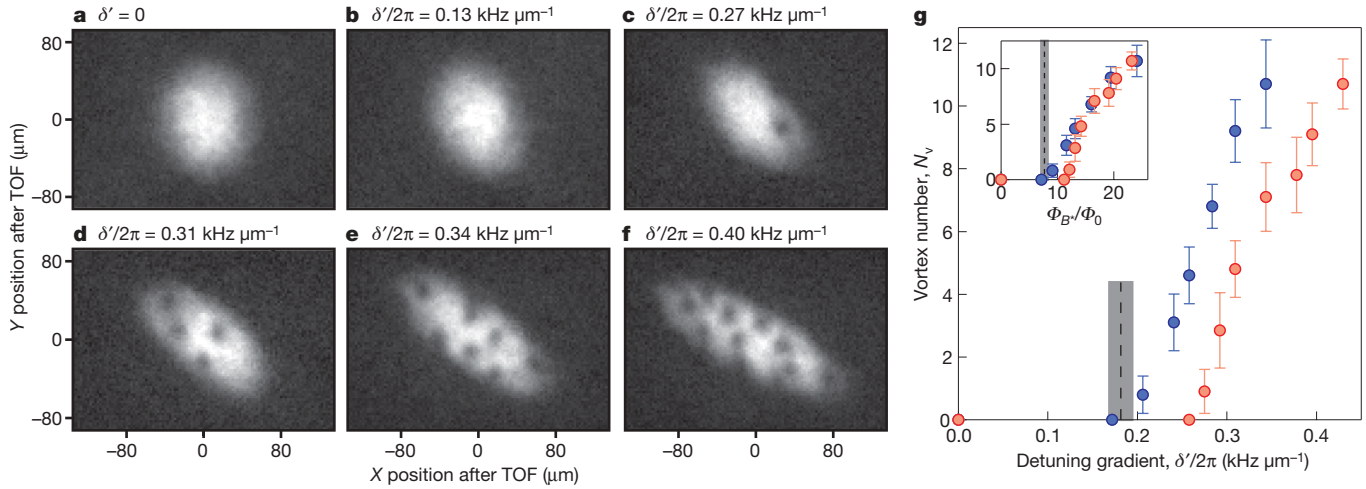

Figure 2 | Appearance of vortices at different detuning gradients. Data was taken for $N = 1.4 \times 10^5$ atoms at hold time $t_h = 0.57$ s. **a–f**, Images of the $|m_F = 0\rangle$ component of the dressed state after a 25.1-ms TOF with detuning gradient $\delta'/2\pi$ from 0 to 0.43 kHz μm^{-1} at Raman coupling $\hbar\Omega_R = 8.20E_L$. **g**, Vortex number N_v versus δ' at $\hbar\Omega_R = 5.85E_L$ (blue circles) and $8.20E_L$ (red circles). Each data point is averaged over at least 20 experimental realizations, and the uncertainties represent one standard deviation σ. The inset displays N_v versus the synthetic magnetic flux $\Phi_{B^*}/\Phi_0 = \mathcal{A}q^*\langle B^*\rangle/h$ in the BEC. The dashed lines indicate δ', below which vortices become energetically unfavourable according to our GPE computation, and the shaded regions show the 1σ uncertainty from experimental parameters.

vortices did not form a lattice and the positions of the vortices were irreproducible between different experimental realizations, consistent with our GPE simulations. We measured N_v as a function of detuning gradient δ' at two couplings, $\hbar\Omega_R = 5.85E_L$ and $8.20E_L$ (Fig. 2). For each Ω_R, vortices appeared above a minimum gradient when the corresponding field $\langle B^*\rangle = \delta'\langle \partial A_x^*/\partial\delta\rangle$ exceeded the critical field B_c^*. (For our coupling, B^* is only approximately uniform over the system and $\langle B^*\rangle$ is the field averaged over the area of the BEC.) The inset shows N_v for both values of Ω_R plotted versus $\Phi_{B^*}/\Phi_0 = \mathcal{A}q^*\langle B^*\rangle/h$, the vortex number for a system of area $\mathcal{A} = \pi R_x R_y$ with the asymptotic vortex density, where R_x (or R_y) is the Thomas–Fermi radius along $\hat{x}$ (or $\hat{y}$). The system size, and thus B_c^*, are approximately independent of Ω_R, so we expected this plot to be nearly independent of Raman coupling. Indeed, the data for $\hbar\Omega_R = 5.85E_L$ and $8.20E_L$ only deviated for $N_v < 5$, probably owing to the intricate dynamics of vortex nucleation[27].

Figure 3 illustrates a progression of images showing that vortices nucleate at the system's edge, fully enter to an equilibrium density and then decay along with the atom number. The timescale for vortex nucleation depends weakly on B^*, and is more rapid for larger B^* with more vortices. It is about 0.3 s for vortex number $N_v \geq 8$, and increases to about 0.5 s for $N_v = 3$. For $N_v = 1$ (B^* near B_c^*), the single vortex always remains near the edge of the BEC. In the dressed state, spontaneous emission from the Raman beams removes atoms from the trap, causing the population to decay with a 1.4(2)-s lifetime, and the equilibrium vortex number decreases along with the area of the BEC.

To verify that the dressed BEC has reached equilibrium, we prepared nominally identical systems in two different ways. First, we varied the initial atom number and measured N_v as a function of atom number N at a fixed hold time of $t_h = 0.57$ s. Second, starting with a large atom number, we measured both N_v and N, as they

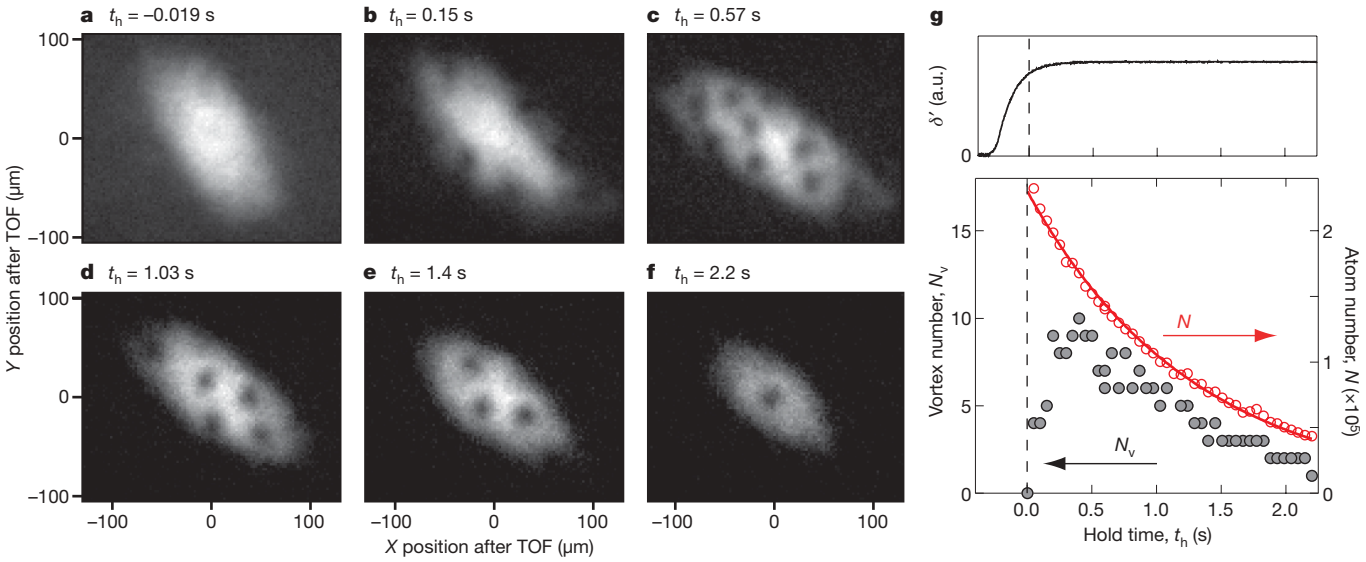

Figure 3 | Vortex formation. **a–f**, Images of the $|m_F = 0\rangle$ component of the dressed state after a 30.1-ms TOF for hold times t_h between -0.019 s and 2.2 s. The detuning gradient $\delta'/2\pi$ is ramped to 0.31 kHz μm^{-1} at the coupling $\hbar\Omega_R = 5.85E_L$. **g**, Top panel shows time sequence of δ'. (a.u., arbitrary units.) Bottom panel shows vortex number N_v (solid symbols) and atom number N (open symbols) versus t_h with a population lifetime of 1.4(2) s. The number in parentheses is the uncorrelated combination of statistical and systematic 1σ uncertainties.

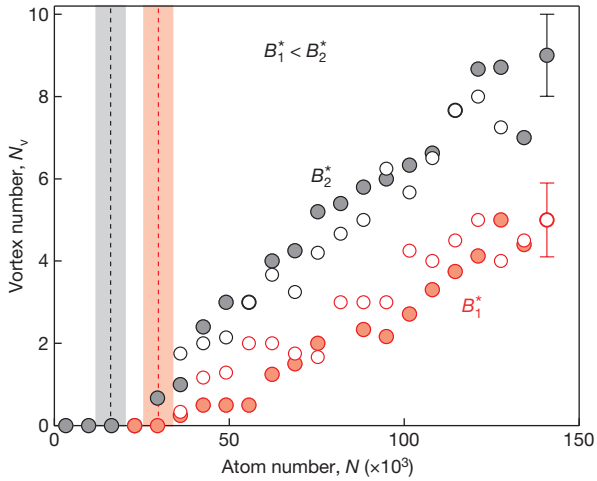

Figure 4 | Equilibrium vortex number. Vortex number N_v versus atom number N at detuning gradient $\delta_1'/2\pi = 0.26$ kHz μm^{-1} (red circles) and $\delta_2'/2\pi = 0.31$ kHz μm^{-1} (black circles), corresponding to synthetic fields $B_1^* < B_2^*$, at Raman coupling $\hbar\Omega_R = 5.85E_L$. The two data points with the largest N show representative 1σ uncertainties, estimated from data in Fig. 2g. We vary N by its initial value with a fixed hold time $t_h = 0.57$ s (solid symbols), and by t_h with a fixed initial N (open symbols). The vertical dashed lines indicate N, below which vortices become energetically unfavourable computed using our GPE simulation. The shaded regions reflect the 1σ uncertainties from the experimental parameters.

decrease with t_h (Fig. 3). Figure 4 compares N_v versus N measured with both methods, each at two detuning gradients corresponding to fields $B_1^* < B_2^*$. The data show that N_v as a function of N is the same for these preparation methods, providing evidence that for $t_h \geq 0.57$ s, N_v has reached equilibrium. As the atom number N falls, the last vortex departs the system when the critical field—increasing with decreasing N—surpasses the actual field.

In conclusion, we have demonstrated optically synthesized magnetic fields for neutral atoms resulting from the Berry's phase, a fundamental concept in physics. This novel approach differs from experiments with rotating gases, in which it is difficult to add optical lattices and rotation is limited by heating, metastability, and the difficulty of adding large angular momentum, preventing access to the quantum-Hall regime. A standout feature in our approach is the ease of adding optical lattices. For example, the addition of a two-dimensional (2D) lattice makes it immediately feasible to study the fractal energy levels of the Hofstadter butterfly[28]. Further, a one-dimensional lattice can divide the BEC into an array of 2D systems normal to the field. A suitable lattice configuration allows access to the $\nu \approx 1$ quantum-Hall regime, with an ensemble of 2D systems each with approximately 200 atoms, and with a realistic interaction energy of about $k_B \times 20$ nK.

METHODS SUMMARY

Dressed state preparation. We created a ^{87}Rb BEC in a crossed dipole trap[29], with $N \approx 4.7 \times 10^5$ atoms in $|F = 1, m_F = -1\rangle$. The quadratic Zeeman shift was $\hbar\varepsilon = 0.61E_L$ for $\omega_Z/2\pi = g\mu_B B/h \approx 2.71$ MHz, where g is the Landé g-factor. To maintain $\delta = 0$ at the BEC's centre as we ramped the field gradient b', we changed $g\mu_B B_0$ by as much as $7E_L$. Simultaneously, we decreased the dipole beam power by 20%, producing our approximately 40-Hz trap frequency along $\hat{x}$. Additionally, the detuning gradient $\delta'\hat{y}$ made the scalar potential V' anti-trapping along $\hat{y}$, reducing f_y from 70 Hz to 50 Hz for our largest δ'. Spontaneous emission from the Raman beams decreased the atom number to $N \approx 2.5 \times 10^5$ for $t_h = 0$, with a condensate fraction of 0.85.

Numerical method. We compared our data to a finite temperature 2D stochastic GPE[30] simulation including the dressed state dispersion $E(k_x, y)$ that depends on y through the detuning gradient δ'. We evolved the time-dependent projected GPE:

$$i\hbar\frac{\partial\psi(\mathbf{x},t)}{\partial t} = \mathcal{P}\left\{\left[E\left(-i\hbar\frac{\partial}{\partial x}, y\right) - \frac{\hbar^2}{2m}\frac{\partial^2}{\partial y^2} + g_{2D}|\psi(\mathbf{x},t)|^2\right]\psi(\mathbf{x},t)\right\}$$

$\mathcal{P}$ projects onto a set of significantly occupied modes, and g_{2D} parameterizes the 2D interaction strength. The stochastic GPE models interactions between the highly occupied modes described by ψ and sparsely occupied thermal modes with dissipation and an associated noise term. We approximately accounted for the finite extent along $\hat{z}$ by making g_{2D} depend on the local 2D density. For low temperatures this 2D model correctly recovers the three-dimensional Thomas–Fermi radii, and gives the expected 2D density profile. These quantitative details are required to compute correctly the critical field or number for the first vortex to enter the system, which are directly tied to the 2D condensate area.

Received 7 August; accepted 20 October 2009.

1. Greiner, M., Mandel, O., Esslinger, T., Hänsch, T. W. & Bloch, I. Quantum phase transition from a superfluid to a Mott insulator in a gas of ultracold atoms. *Nature* **415**, 39–44 (2003).
2. Regal, C. A., Greiner, M. & Jin, D. S. Observation of resonance condensation of fermionic atom pairs. *Phys. Rev. Lett.* **92**, 040403 (2004).
3. Zwierlein, M. W. *et al.* Condensation of pairs of fermionic atoms near a Feshbach resonance. *Phys. Rev. Lett.* **92**, 120403 (2004).
4. Tsui, D. C., Stormer, H. L. & Gossard, A. C. Two-dimensional magnetotransport in the extreme quantum limit. *Phys. Rev. Lett.* **48**, 1559–1562 (1982).
5. Laughlin, R. B. Anomalous quantum Hall effect: an incompressible quantum fluid with fractionally charged excitations. *Phys. Rev. Lett.* **50**, 1395–1398 (1983).
6. Zwierlein, M. W., Abo-Shaeer, J. R., Schirotzek, A., Schunck, C. H. & Ketterle, W. Vortices and superfluidity in a strongly interacting Fermi gas. *Nature* **435**, 1047–1051 (2005).
7. Schweikhard, V., Coddington, I., Engels, P., Mogendorff, V. P. & Cornell, E. A. Rapidly rotating Bose-Einstein condensates in and near the lowest Landau level. *Phys. Rev. Lett.* **92**, 040404 (2004).
8. Madison, K. W., Chevy, F., Wohlleben, W. & Dalibard, J. Vortex formation in a stirred Bose-Einstein condensate. *Phys. Rev. Lett.* **84**, 806–809 (2000).
9. Abo-Shaeer, J. R., Raman, C., Vogels, J. M. & Ketterle, W. Observation of vortex lattices in Bose-Einstein condensates. *Science* **292**, 476–479 (2001).
10. Juzeliūnas, G. & Öhberg, P. Slow light in degenerate Fermi gases. *Phys. Rev. Lett.* **93**, 033602 (2004).
11. Jaksch, D. & Zoller, P. Creation of effective magnetic fields in optical lattices: the Hofstadter butterfly for cold neutral atoms. *N. J. Phys.* **5**, 56.1–56.11 (2003).
12. Sorensen, A. S., Demler, E. & Lukin, M. D. Fractional quantum Hall states of atoms in optical lattices. *Phys. Rev. Lett.* **94**, 086803 (2005).
13. Berry, M. V. Quantal phase factors accompanying adiabatic changes. *Proc. R. Soc. Lond. A* **392**, 45–57 (1984).
14. Juzeliūnas, G., Ruseckas, J., Öhberg, P. & Fleischhauer, M. Light-induced effective magnetic fields for ultracold atoms in planar geometries. *Phys. Rev. A* **73**, 025602 (2006).
15. Gunter, K. J., Cheneau, M., Yefsah, T., Rath, S. P. & Dalibard, J. Practical scheme for a light-induced gauge field in an atomic Bose gas. *Phys. Rev. A* **79**, 011604 (2009).
16. Spielman, I. B. Raman processes and effective gauge potentials. *Phys. Rev. A* **79**, 063613 (2009).
17. Nayak, C., Simon, S. H., Stern, A., Freedman, M. & Sarma, S. D. Non-abelian anyons and topological quantum computation. *Rev. Mod. Phys.* **80**, 1083–1159 (2008).
18. Radu, I. P. *et al.* Quasi-particle properties from tunneling in the formula fractional quantum Hall state. *Science* **320**, 899–902 (2008).
19. Cooper, N. R. Rapidly rotating atomic gases. *Adv. Phys.* **57**, 539–616 (2008).
20. Cheneau, M. *et al.* Geometric potentials in quantum optics: A semi-classical interpretation. *Europhys Lett.* **83**, 60001 (2008).
21. Leanhardt, A. E. *et al.* Imprinting vortices in a Bose-Einstein condensate using topological phases. *Phys. Rev. Lett.* **89**, 190403 (2002).
22. Andersen, M. F. *et al.* Quantized rotation of atoms from photons with orbital angular momentum. *Phys. Rev. Lett.* **97**, 170406 (2006).
23. Matthews, M. R. *et al.* Vortices in a Bose-Einstein condensate. *Phys. Rev. Lett.* **83**, 2498–2501 (1999).
24. Lin, Y.-J. *et al.* Bose-Einstein condensate in a uniform light-induced vector potential. *Phys. Rev. Lett.* **102**, 130401 (2009).
25. Yarmchuk, E. J., Gordon, M. J. V. & Packard, R. E. Observation of stationary vortex arrays in rotating superfluid helium. *Phys. Rev. Lett.* **43**, 214–217 (1979).
26. Lundh, E., Pethick, C. J. & Smith, H. Zero-temperature properties of a trapped Bose-condensed gas: beyond the Thomas-Fermi approximation. *Phys. Rev. A* **55**, 2126–2131 (1997).
27. Murray, D. R., Öhberg, P., Gomila, D. & Barnett, S. M. Vortex nucleation in Bose-Einstein condensates due to effective magnetic fields. *Phys. Rev. A* **79**, 063618 (2009).
28. Hofstadter, D. R. Energy levels and wave functions of Bloch electrons in rational and irrational magnetic fields. *Phys. Rev. B* **14**, 2239–2249 (1976).
29. Lin, Y.-J., Perry, A. R., Compton, R. L., Spielman, I. B. & Porto, J. V. Rapid production of ^{87}Rb Bose-Einstein condensates in a combined magnetic and optical potential. *Phys. Rev. A* **79**, 063631 (2009).
30. Blakie, P. B., Bradley, A. S., Davis, M. J., Ballagh, R. J. & Gardiner, C. W. Dynamics and statistical mechanics of ultra-cold Bose gases using c-field techniques. *Adv. Phys.* **57**, 363–455 (2008).

Acknowledgements We thank W. D. Phillips for discussions. This work was partially supported by ONR, ARO with funds from the DARPA OLE programme, and the NSF through the JQI Physics Frontier Center. R.L.C. acknowledges the NIST/NRC postdoctoral programme and K.J.-G. thanks CONACYT.

Author Contributions All authors contributed to writing of the manuscript. Y.-J.L. led the data collection effort (with assistance from R.L.C. and K.J.-G.). I.B.S. and J.V.P. designed the original apparatus, which was largely constructed by I.B.S., and Y.-J.L. implemented the specific changes required for the present experiment. I.B.S. conceived the experiment and performed numerical and analytic calculations. This work was supervised by I.B.S. with consultations from J.V.P.

Author Information Reprints and permissions information is available at www.nature.com/reprints. Correspondence and requests for materials should be addressed to I.B.S. (ian.spielman@nist.gov).